

Field-dependent specific heat of Yb4As3: agreement between a spin-1/2 model and experiment

R. Matysiak, G. Kamieniarz, Philipp Gegenwart, A. Ochiai

Angaben zur Veröffentlichung / Publication details:

Matysiak, R., G. Kamieniarz, Philipp Gegenwart, and A. Ochiai. 2009.
"Field-dependent specific heat of Yb4As3: agreement between a spin-1/2 model
and experiment." *Physical Review B* 79 (22): 224413.
<https://doi.org/10.1103/physrevb.79.224413>.



Field-dependent specific heat of Yb_4As_3 : Agreement between a spin- $\frac{1}{2}$ model and experiment

R. Matysiak*

Institute of Engineering and Computer Education, University of Zielona Góra, ul. prof. Z. Szafrana 4, 65-516 Zielona Góra, Poland

G. Kamieniarz†

*Computational Physics Division, Faculty of Physics, A. Mickiewicz University, ul. Umultowska 85, 61-614 Poznań, Poland
and Max Planck Institute for the Physics of Complex Systems, 01187 Dresden, Germany*

P. Gegenwart

I. Physikalisches Institut, Georg-August-Universität Göttingen, Friedrich-Hund-Platz 1, 37077 Göttingen, Germany

A. Ochiai

Center for Low Temperature Science, Tohoku University, Sendai 980-8578, Japan

(Received 1 February 2009; revised manuscript received 17 May 2009; published 12 June 2009)

We report the low-temperature specific-heat measurements on polydomain Yb_4As_3 at magnetic fields up to 20 T. Taking into account the Bethe ansatz results, the zero-field data have been used for the estimation of the lattice specific heat, resulting in a value of the exchange integral for the Heisenberg model of the antiferromagnetic spin $S=\frac{1}{2}$ chain of $J/k_B=-28$ K. A quantitative agreement has been achieved between the experimental magnetic specific-heat data in magnetic field and the numerical results obtained by the quantum transfer-matrix (QTM) simulation technique. The finite-size QTM approximants have been analyzed and an extrapolation procedure recovering the known density matrix renormalization group (DMRG) results down to very low temperature has been proposed. On the basis of the data in magnetic field and using the earlier DMRG results, the energy-gap size Δ has been analyzed as a function of the applied magnetic field B , leading to an experimental verification of the scaling law $\Delta \propto B^{2/3}$ following from the sine-Gordon model.

DOI: [10.1103/PhysRevB.79.224413](https://doi.org/10.1103/PhysRevB.79.224413)

PACS number(s): 75.10.Jm, 75.40.Cx, 75.40.Mg, 71.55.Ak

I. INTRODUCTION

The problems related to one-dimensional (1D) magnetism have generated unceasing interests for both theoreticians and experimentalists. Theoretical description of such simple systems is less complex than those of higher dimensions and still their analysis is very useful for comprehension of phenomena taking place in two-dimensional and three-dimensional systems and for evaluation of the approximations used for descriptions of the systems of higher dimensions. Moreover, theoretical models of low-dimensional systems have increasingly often been confirmed in real chemical compounds.¹ Particularly important have become the results obtained on the basis of Bethe ansatz (BA),² and the theoretical analysis of the systems with integer spin showing the presence of the energy gap between the ground state and the lowest-excited states,³ which has been realized in real systems.⁴ The compound studied in this work Yb_4As_3 exemplifies systems with the energy gap being a consequence of the effect of staggered magnetic field as has been evidenced by the sine-Gordon model.⁵

The role of computer simulations in investigation of the low-dimensional quantum spin systems has recently increased as a result of progress in the methods of simulations and increasing computer power.⁶⁻⁸ The restriction to the low dimensions of the systems studied is imposed by the complexity of the algorithms used. However, for the spin chains the simulation methods have brought reliable results of high accuracy,⁸⁻¹⁰ which can be verified on the basis of the exact theoretical solutions and can be used to verify the approximate theoretical results.

At high temperatures, Yb_4As_3 is a homogeneous intermediate valent (IV) metal with a valence ratio of $\text{Yb}^{2+}/\text{Yb}^{3+}=3:1$. Three quarters of the Yb ions have filled $4f$ shells with the valency $2+$ and one quarter with the valency $3+$ has one hole in the f shell. Above the charge-ordering (CO) temperature $T_{\text{CO}} \approx 295$ K the holes in the f shells move between the Yb ions due to the hybridization with the As- $4p$ holes. Yb_4As_3 belongs to a family of R_4X_3 (R =rare earth and X =As, Bi, P, Sb) compounds of the anti Th_3P_4 structure.¹¹ The Yb ions occupy the phosphorus sites at the threefold symmetry axes and the As ions are located at the thorium sites. This compound has a cubic crystal structure with the lattice constant $a=8.788$ Å in which the Yb ions reside statistically on four equivalent families of chains along the space diagonals of a cube.¹²

At $T_{\text{CO}} \approx 295$ K, a first-order structural phase transition has been observed which is accompanied by discontinuities of the electrical resistivity and the Hall coefficient.¹¹ Below $T_{\text{CO}} \approx 295$ K, the crystal Yb_4As_3 shrinks along the $\langle 111 \rangle$ direction getting a trigonal structure (the trigonal angle is 90.8°). The polarized neutron-diffraction study has shown that the Yb ions occupying the sites aligned along the shrinking $\langle 111 \rangle$ direction become trivalent and the rest of Yb ions are divalent.¹³ At low temperatures, Yb_4As_3 is semimetallic with extremely low carrier concentration of 10^{-3} As $4p$ holes per f.u.¹⁴ The Yb^{3+} ions have one hole in the $4f$ closed shell and form a one-dimensional spin $S=\frac{1}{2}$ chain along the $\langle 111 \rangle$ direction. The remaining Yb ions occupy nonmagnetic divalent states. The $J=7/2$ ground-state multiplet splits into four doublets as a result of the crystal-field effect. Thus, the low-

temperature dynamics is described by an effective $S=\frac{1}{2}$ spin chain. The neutron-scattering experiments on Yb_4As_3 have actually confirmed that the excitation spectrum is well described by the one-dimensional $S=\frac{1}{2}$ isotropic Heisenberg model¹⁵ in the absence of a magnetic field. The interchain interactions are small and ferromagnetic, leading to a low- T spin-glass freezing.¹⁶

At low temperatures and in the absence of a magnetic field, the system exhibits a heavy-fermion-like behavior with a linear specific-heat coefficient $\gamma \approx 200$ [mJ/(K² mol)], which has later been attributed to 1D spin excitations in the Yb^{3+} antiferromagnetic Heisenberg chains.^{16,17} However, as shown by the neutron-scattering experiment under magnetic field, a gap in the spin excitation spectrum of Yb_4As_3 opens and obeys a power-law dependence $B^{2/3}$,¹⁸ which gives a strong experimental evidence for the existence of a staggered field alternating along the Yb^{3+} chains induced by the Dzyaloshinskii-Moriya interaction as suggested by the sine-Gordon model⁵ and observed also in copper benzoate¹⁹ and copper pyrimidine complex.²⁰ The system seems also interesting as a candidate for the anomalous electron-spin-resonance behavior.^{21,22}

The gap opening also affects the field-dependent specific heat at low temperatures. The values of the specific-heat coefficient are strongly reduced with respect to the zero-field results and in $C(T)/T$ some maxima related to the gap opening are found.^{18,23}

However, the experimental specific-heat results have not been quantitatively explained within the Heisenberg model with the staggered field yet. Previous calculations²⁴ have systematically overestimated the experimental specific-heat data and some deviations from the power-law behavior of the energy gap have been observed.²³ These discrepancies are addressed in this paper.

II. EXPERIMENTAL DETAILS

The experiments have been carried out on a 20 mg high-quality single crystal of Yb_4As_3 , prepared as described previously.¹¹ The specific heat has been obtained by the relaxation technique using a commercial microcalorimeter from Oxford Instruments in combination with a superconducting 20 T magnet. A miniaturized Cernox chip resistor, calibrated by Oxford Instruments in magnetic field has been used. The trigonal lattice distortion accompanying the charge ordering transition results in a polydomain low- T structure. We have applied the magnetic field parallel to one of the four equivalent cubic space diagonals.

III. MODEL AND THE TRANSFER-MATRIX SIMULATION TECHNIQUE

Computer modeling of the finite-temperature properties of the Yb_4As_3 is based on the $S=\frac{1}{2}$ anisotropic Heisenberg model with the antisymmetric Dzyaloshinskii-Moriya interaction^{25,26}

$$\mathcal{H} = - \left\{ J \sum_{i=1}^N [\hat{S}_i^z \hat{S}_{i+1}^z + \cos(2\theta) (\hat{S}_i^x \hat{S}_{i+1}^x + \hat{S}_i^y \hat{S}_{i+1}^y)] + J \sin(2\theta) \sum_{i=1}^N (-1)^i (\hat{S}_i^x \hat{S}_{i+1}^y - \hat{S}_i^y \hat{S}_{i+1}^x) + g_{\perp} \mu_B B \sum_{i=1}^N \hat{S}_i^x \right\}. \quad (1)$$

The Dzyaloshinskii-Moriya interaction is eliminated by rotating the spins in the x - y plane by the angle θ ,⁸

$$\begin{aligned} \hat{S}_i^x &= \cos(\theta) S_i^x + (-1)^i \sin(\theta) S_i^y \\ \hat{S}_i^y &= -(-1)^i \sin(\theta) S_i^x + \cos(\theta) S_i^y \\ \hat{S}_i^z &= S_i^z. \end{aligned} \quad (2)$$

Then the model is mapped onto⁸

$$\mathcal{H} = - J \sum_{i=1}^N \mathbf{S}_i \mathbf{S}_{i+1} - g_{\perp} \mu_B B^x \sum_{i=1}^N S_i^x + - g_{\perp} \mu_B B_y^y \sum_{i=1}^N (-1)^i S_i^y, \quad (3)$$

where $B^x = B \cos(\theta)$, $B_y^y = B \sin(\theta)$, and B is the uniform external magnetic field perpendicular to the one-dimensional spin chain. Equation (3) describes the effective isotropic Heisenberg model with both the uniform field B^x and the transverse staggered field B_y^y . If the external magnetic field is applied along the spin chain then $\theta=0$ and $g_{\perp} = g_{\parallel}$ in Eq. (3). So far the thermodynamical properties of the compound Yb_4As_3 have been described by the model (3) using the following parameters²⁴

$$J/k_B = -26 \text{ K}, \quad g_{\parallel} = 2.9, \quad g_{\perp} = 1.3, \quad \tan(\theta) = 0.19.$$

The thermodynamical mean value of any quantity described by the self-adjoint operator \mathcal{A} is given by

$$\langle \mathcal{A} \rangle = \frac{1}{\mathcal{Z}} \text{Tr} \{ \mathcal{A} e^{-\beta \mathcal{H}} \}, \quad \beta = \frac{1}{k_B T}, \quad (4)$$

where k_B is the Boltzmann constant and T is the temperature in K . We can also calculate the thermodynamic properties from the derivatives of the free energy related to the partition function \mathcal{Z} . For the spin system described in Eq. (3) we can calculate the canonical partition function \mathcal{Z} from the definition

$$\mathcal{Z} = \text{Tr} e^{-\beta \mathcal{H}}. \quad (5)$$

The values of matrix elements of $e^{-\beta \mathcal{H}}$ cannot be calculated for large N because of noncommuting operators in Eq. (3). Thus, to eliminate this restriction, we look for systematic approximants to the partition function \mathcal{Z} .

We express the Hamiltonian (3) as a sum of the spin-pair operators $\mathcal{H}_{i,i+1}$, where

$$\begin{aligned} \mathcal{H}_{i,i+1} &= - J \mathbf{S}_i \mathbf{S}_{i+1} - \frac{1}{2} g_{\perp} \mu_B B^x (S_i^x + S_{i+1}^x) \\ &+ - \frac{1}{2} g_{\perp} \mu_B (-1)^i B_y^y (S_i^y - S_{i+1}^y). \end{aligned} \quad (6)$$

In the checker-board decomposition (CBD) we divide the Hamiltonian (3) into two noncommuting parts⁷

$$\begin{aligned}\mathcal{H} &= \mathcal{H}^{odd} + \mathcal{H}^{even} \\ &= (\mathcal{H}_{1,2} + \dots + \mathcal{H}_{N-1,N}) \\ &\quad + (\mathcal{H}_{2,3} + \dots + \mathcal{H}_{N,1}),\end{aligned}\quad (7)$$

where each part is defined by the commuting spin-pair operators $\mathcal{H}_{i,i+1}$. Then the series of the classical approximants of the quantum thermal values can be found using the general Suzuki-Trotter formula.⁷ The partition function is calculated from the expression

$$\mathcal{Z} = \lim_{m \rightarrow \infty} \mathcal{Z}_m = \lim_{m \rightarrow \infty} \text{Tr} \left[\prod_{i=1}^{N/2} \mathcal{V}_{2i-1,2i} \prod_{i=1}^{N/2} \mathcal{V}_{2i,2i+1} \right]^m, \quad (8)$$

where $\mathcal{V}_{i,i+1} = e^{-\beta \mathcal{H}_{i,i+1}/m}$, $i=1,2,\dots,N$, and m is a natural number (referred to as the Trotter number).

The approximant \mathcal{Z}_m can be calculated numerically without any restrictions on the value of N , by the quantum transfer-matrix (QTM) method. The computation of \mathcal{Z}_m is possible for relatively small values of m , because of computer storage limitation, but the leading errors in taking a finite m approximant are on the order of $1/m^2$ and therefore, extrapolations to $m \rightarrow \infty$ can be performed.

For infinite chains (the macroscopic limit) it is better to reverse the transfer direction and to calculate the partition function from the largest eigenvalue of the transfer matrix. In order to reverse the transfer direction we must define a new local transfer matrix $\mathcal{L}_{r,r+1}$ whose elements depend on the local transfer-matrix $\mathcal{V}_{i,i+1}$ elements

$$\langle S_{r,i}^z S_{r+1,i}^z | \mathcal{L}_{r,r+1} | S_{r,i+1}^z S_{r+1,i+1}^z \rangle = \langle S_{r,i}^z S_{r,i+1}^z | \mathcal{V}_{i,i+1} | S_{r+1,i}^z S_{r+1,i+1}^z \rangle. \quad (9)$$

These operators act in a Hilbert space \mathcal{H}^{2m} whose dimension is independent of N .

Now we define a unitary shift operator. In the case of the nonuniform spin chains we define also a unitary shift operator \mathcal{D} , acting in the space \mathcal{H}^{2m} which is a direct product of $2m$ single-spin spaces \mathcal{H}^2 , similarly to that for the uniform chain⁷

$$\mathcal{D} \equiv \sum_{S_1^z} \dots \sum_{S_{2m}^z} |S_3^z \dots S_{2m}^z S_1^z S_2^z\rangle \langle S_1^z S_2^z S_3^z \dots S_{2m}^z|. \quad (10)$$

Using Eq. (10) we can express the operators $\mathcal{L}_{r,r+1}$ in terms of the operators $\mathcal{L}_{1,2}$ and $\mathcal{L}_{2,3}$

$$\begin{aligned}\mathcal{L}_{2r-1,2r} &= (\mathcal{D}^+)^{r-1} \mathcal{L}_{1,2} \mathcal{D}^{r-1}, \\ \mathcal{L}_{2r,2r+1} &= (\mathcal{D}^+)^{r-1} \mathcal{L}_{2,3} \mathcal{D}^{r-1}.\end{aligned}\quad (11)$$

In this case the global transfer matrices can be expressed in terms of two operators $\mathcal{L}_{1,2}$ and $\mathcal{L}_{2,3}$,

$$\mathcal{W}_r = (\mathcal{L}_{r,r+1} \mathcal{D}^+)^m, \quad r=1,2. \quad (12)$$

Finally, the m th classical approximant to the partition function can be written in the following form:

$$\mathcal{Z}_m = \text{Tr}(\mathcal{W}_1 \mathcal{W}_2)^{N/2}. \quad (13)$$

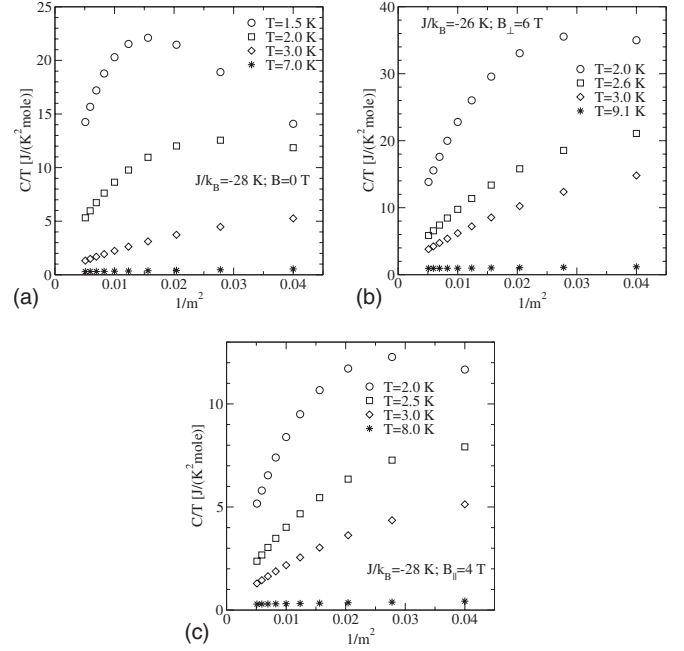


FIG. 1. Specific heat as a function of $1/m^2$ for different temperatures and magnetic field intensities: (a) $B_{\perp}=0$ T; (b) $B_{\perp}=6$ T; and (c) $B_{\parallel}=4$ T.

In the limit $N \rightarrow \infty$ the partition function \mathcal{Z} is equal to the highest eigenvalue of the global transfer matrix $\mathcal{W} = \mathcal{W}_1 \mathcal{W}_2$.

IV. DESCRIPTION OF THE EXTRAPOLATION PROCEDURE

The fundamental assumptions of the QTM technique have been described above. As follows from them, in order to obtain a certain value of specific heat or any other thermodynamical quantity calculated from the partition function [Eq. (13)], one should analyze for a given temperature the dependence of the calculated specific heat on Trotter index m and extrapolate the dependence $C(1/m^2)$ in the limit $m \rightarrow \infty$. Figures 1(a)–1(c) present the numerical results of $C/T(1/m^2)$ obtained without an external magnetic field [Fig. 1(a)] and in the presence of an applied magnetic field B_{\perp} perpendicular to the direction of the chain [Fig. 1(b)] and B_{\parallel} parallel to it [Fig. 1(c)]. Each figure shows the plots for different temperatures, assuming $J/k_B = -28$ K or $J/k_B = -26$ K as defined in the legend. For high temperatures the dependence $C(1/m^2)$ is linear in the whole range of the Trotter index values (e.g., $T=8$ K) as shown in Figs. 1(a)–1(c). Moreover, the specific-heat changes with increasing m are small, so the extrapolation results are very accurate in these conditions. For low temperatures ($T < 4$ K) the dependence $C(1/m^2)$ significantly deviates from linear character and with increasing m the specific-heat values change substantially, so the accuracy of the estimated specific heat is affected and more careful extrapolation analysis is needed.

In order to improve the accuracy of the extrapolation for low temperatures, the analysis of the specific heat as a function of $1/m^2$ was made as follows. A function described

by the extrapolation polynomial of the degree k ($k = 1, \dots, k_{\max}$)

$$C_m/T = \sum_{j=0}^k a_j \cdot \left(\frac{1}{m^2}\right)^j \quad (14)$$

was developed to approximants C_m corresponding to $m_{\min} \leq m \leq m_{\max}$. For practical reasons, in our procedure $k_{\max} \leq 10$. The value of the highest Trotter index m_{\max} is fixed and amounts to 14 or 15 in low temperatures and 13 in high temperatures. The value m_{\min} is subject to variation in the region $2 \leq m_{\min} \leq m_{\max} - 1$.

The extrapolation procedure starts with $m_{\min} = 2$ and is continued till $m = m_{\max} - 1$. In each step the number of fitted points n ($n = m_{\max} - m_{\min} + 1$) is fixed and a number of extrapolations are performed with polynomials of the degree k ($1 \leq k \leq n - 1$, but not more than 10). In this way for a given field and temperature we obtain a set of extrapolated values for different values of n and k and we can present the variation in the data with n for the fixed degree k of the polynomial.

The results of the analysis of the extrapolated specific-heat values according to the above procedure are shown in Figs. 2(a)–2(f). The first two plots, Figs. 2(a) and 2(b), correspond to the condition of zero magnetic field and two different temperatures ($T = 1.5$ K and $T = 3.0$ K). To check the accuracy of the extrapolations performed the plots were referred to the value obtained on the basis of the Bethe ansatz approach² which is shown as a dotted line in Figs. 2(a) and 2(b). As shown, the convergence depends significantly on the degree k of the polynomial. The curves corresponding to $k = 1$ cannot be shown here because they are beyond the scale in Figs. 2(a)–2(f). The convergence of the extrapolated values is much better for higher temperatures [$T = 3$ K, Fig. 2(b)] and implies higher accuracy of the numerical estimates.

The next two figures present the variation in results of the extrapolation for two different temperatures ($T = 2.0$ K and $T = 3.0$ K) and for the field direction perpendicular to the chain. Figures 2(c) and 2(d) give a comparison of the extrapolated results with those obtained by density-matrix renormalization group (DMRG) (Ref. 8) (dotted line). Again, the convergence toward expected DMRG values is improved with increasing value of the polynomial degree k . For $k \geq 4$ and n being small enough, the QTM estimates agree with the DMRG value within 1%. The last two figures show the results of the extrapolation for two different temperatures ($T = 2.0$ K and $T = 3.0$ K) but for the magnetic field direction parallel to the chain. No exact reference data are known but the behavior of the extrapolated data is the same, so that we expect that even down to temperatures $k_B T / J = 0.077$ we can reach accuracy on the order of 1%.

The results of our numerical asymptotic analysis extrapolations and the estimated errors have been compared with the best-known literature values^{2,8} in Table I. For the perpendicular magnetic field, the QTM results are compared with the DMRG ones read off Fig. 9 in Ref. 8. The read off results are given with the errors introduced by the graphical analysis. The above analysis reveals an excellent agreement between our numerical results and those obtained by the other

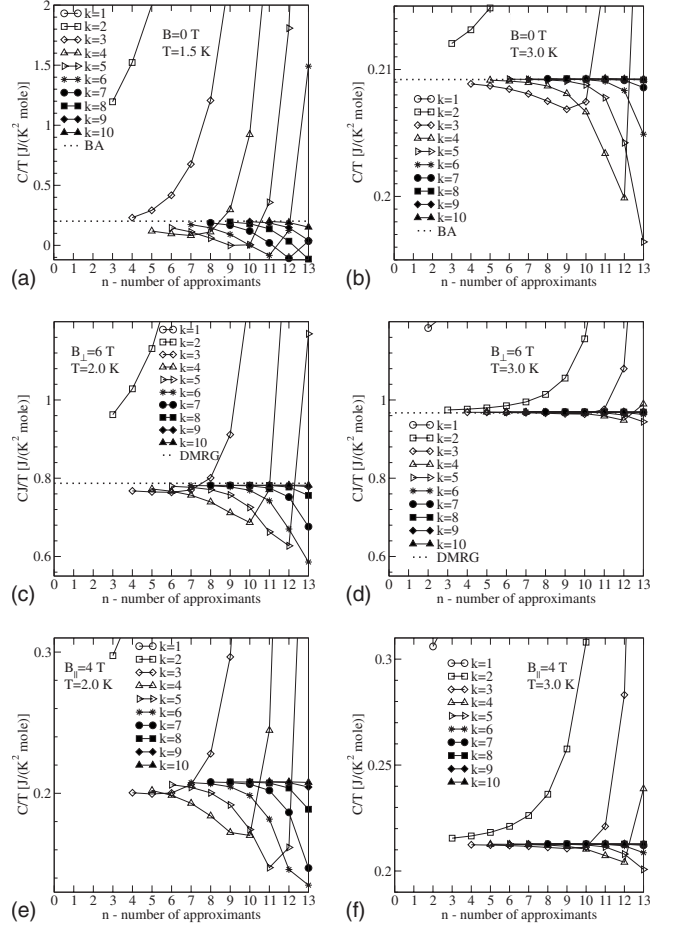


FIG. 2. The extrapolated values of specific heat versus the number of points n for which the polynomials are constructed. Each particular plot corresponds to the polynomial of a given degree k . The figures [(a)–(f)] have been drawn for different magnetic fields: Figs. (a) and (b) for $B = 0$ T, $J/k_B = -28$ K, and the QTM results in reference to the Bethe ansatz results (Ref. 2); Figs. (c) and (d) for $B_{\perp} = 6$ T ($J/k_B = -26$ K) and the QTM results in reference to the DMRG results (Ref. 8); and Figs. (e) and (f) for $B_{\parallel} = 4$ T ($J/k_B = -28$ K), only the QTM results.

two methods: BA (Ref. 2) and DMRG.⁸ The accuracy of the present QTM results is comparable with that of DMRG results for temperatures as low as $T = 2.0$ K, ($k_B T / J = 0.077$) and is better than 1% (the relative error is smaller than 1%). This consideration confirms that our QTM technique is a reliable tool for analysis of the specific-heat measurements of the systems modeled by the Hamiltonian (3).

V. MODELING OF THE POLYDOMAIN SAMPLE USING THE ZERO-FIELD DATA

The zero-field specific-heat data are presented in Fig. 3 as $C(T)/T$. Since the nonmagnetic reference system Lu_4As_3 does not show a charge ordering accompanied by a lattice distortion, it could not be used as reference for the phonon contribution to the specific heat of Yb_4As_3 . Therefore, we have first estimated the lattice contribution and the exchange coupling J by exploiting the BA results.² The BA method²⁷ is

TABLE I. Comparison between the QTM estimates and the corresponding BA and DMRG results.

$B=0$ T, $J/k_B=-28$ K			$B_{\perp}=6$ T, $J/k_B=-26$ K		
T [K]	$C/T(\text{BA})$ [J/(K ² mole)]	$C/T(\text{QTM})$ [J/(K ² mole)]	T [K]	$C J /T(\text{DMRG})$ [J/K]	$C J /T(\text{QTM})$ [J/K]
1.5	0.2014085	0.200 ± 0.002	2.0	0.787 ± 0.010	0.782 ± 0.001
2.0	0.2033790	0.2034 ± 0.0001	2.6	0.944 ± 0.005	0.9474 ± 0.0002
3.0	0.2092113	0.2093 ± 0.0001	3.0	0.967 ± 0.005	0.9694 ± 0.0001
7.0	0.2586549	0.25865 ± 0.00003	9.1	0.902 ± 0.005	0.90255 ± 0.00001

exact and can be used to calculate the thermodynamic properties of the $S=\frac{1}{2}$ Heisenberg spin chain. The experimental specific heat C_{exp} is a sum of two components: the magnetic and the lattice specific heat. The magnetic part depends on J , its temperature behavior was found within the BA approach² and can be fitted by the Pade approximants listed in Table I of Ref. 2. The agreement of this approximation with BA in the temperature range $0.01 \leq k_B T/J \leq 5$ is estimated to be $0.5 \cdot 10^{-4}\%$.² On the basis of the experimental results in zero magnetic field, the lattice contribution to the specific heat C_{ph} in the form

$$C_{\text{ph}} = \alpha T^3 + \beta T^5 \quad (15)$$

can be estimated assuming that the magnetic contribution C_{BA} is given by the BA results for the Heisenberg model in zero magnetic field.²

As shown in Fig. 3, the magnetic contribution to specific-heat coefficient corresponding to $J/k_B=-26$ K and $J/k_B=-27$ K at low temperatures ($T \leq 4$ K) is greater than the experimental data, so these values of the exchange integral cannot be accepted because the lattice contribution to the specific heat obtained would be negative. The lowest acceptable value is $J/k_B=-28$ K which is still consistent with the neutron-scattering data.¹⁸ Having fixed $J/k_B=-28$ K, we fitted the differences $C_{\text{ph}}/T = C_{\text{exp}}/T - C_{\text{BA}}(J/k_B=-28 \text{ K})/T$, and found values of the coefficients in expression (15)

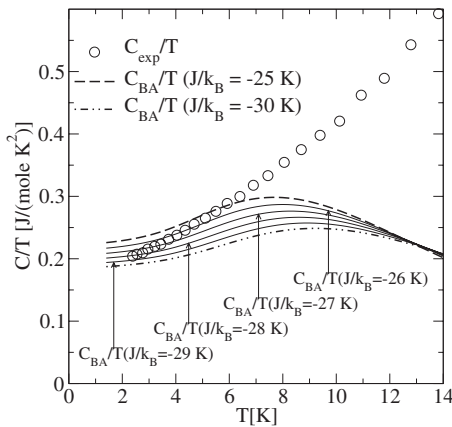


FIG. 3. Temperature dependence of the measured specific-heat coefficient C/T in zero magnetic field plotted using open symbols and a comparison with BA results for different values of the exchange integral.

$$\alpha = 1.11 \times 10^{-3} \text{ [J/(mole K}^4\text{)]}$$

and

$$\beta = 4.9 \times 10^{-6} \text{ [J/(mole K}^6\text{)].}$$

Figure 4 presents the experimental values of the total specific heat, the experimental data minus the estimated contribution of the lattice specific heat (i.e., the magnetic contribution to the specific heat) and the lattice contribution to the specific heat. The experimental values are presented by full and open circles, while the results of numerical and analytical analyses are illustrated by curves of different types.

The estimation of the lattice contribution to the specific heat was based on the experimental results obtained for Yb_4As_3 in a wide range of temperatures 2.5–14 K. From now on, we consider the specific-heat data found from the subtraction of the lattice contribution as the experimental magnetic contribution.

VI. COMPARISON BETWEEN THE MODEL AND EXPERIMENT IN THE PRESENCE OF MAGNETIC FIELD

In our subsequent simulations of the low-temperature specific heat of Yb_4As_3 in external magnetic fields, we assumed

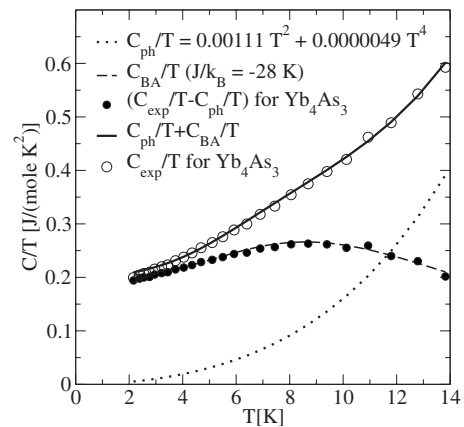


FIG. 4. Temperature dependence of the specific-heat coefficient in zero magnetic field. The experimental results are shown by open circles (polydomain sample) and full circles (after subtraction of the lattice component to specific heat). The lines present the numerical results of the lattice contribution to specific heat (dotted line), the BA results of the magnetic contribution to specific heat for $J/k_B=-28$ K (dashed line), and the sum of these two components (continuous line).

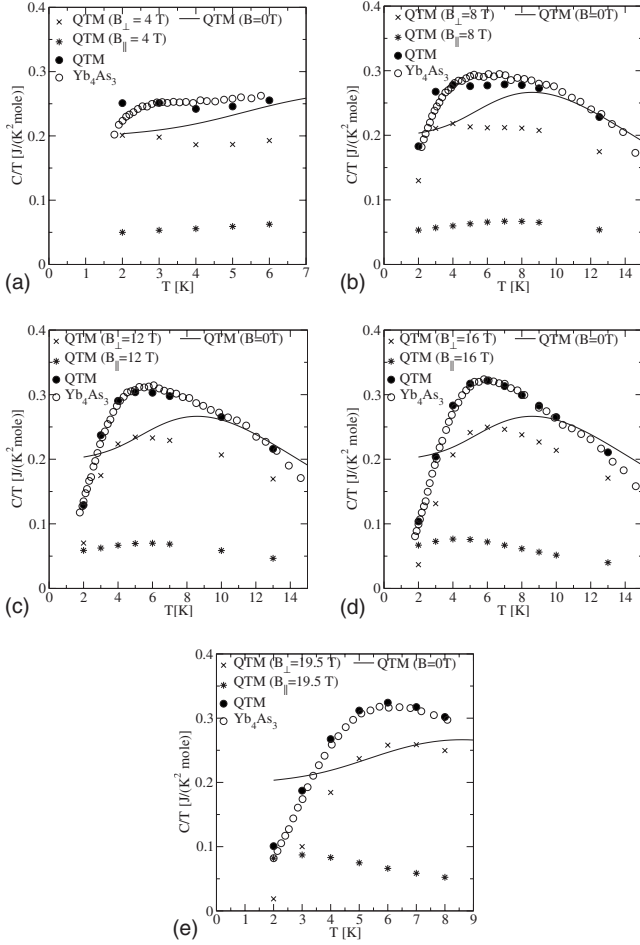


FIG. 5. Temperature dependencies of specific-heat coefficient for different intensities of the magnetic field applied. Open circles correspond to the experimental data while filled circles correspond to the results of the simulations. Also the results for the two components of the field are shown; for the perpendicular (crosses) and parallel (asterisks) components the weights 0.75 and 0.25 have been applied, respectively. The results of the QTM calculations in zero field are shown by continuous line.

the intrachain exchange coupling $J/k_B = -28$ K, while the other parameters in the model Hamiltonian (3) were taken from literature. The g factors parallel and perpendicular to the spin chain of Yb_4As_3 were estimated as $g_{\parallel} = 3.0$ and $g_{\perp} = 1.3$ from the analysis of the inelastic scattering vector dependence of the response in zero field and the magnetic moment induced on the Yb^{3+} ions, measured by polarized neutron diffraction in a magnetic field.¹⁸ As to the transformation angle, the magnetization measurements led to the value $\tan(\theta) = 0.19$ (Ref. 8) so that the uniform field was about five times stronger than the effective staggered field induced by the Dzyaloshinskii-Moriya interaction. The experimental data for the field-dependent specific-heat coefficient have been reported elsewhere.²⁴ Here we have reanalyzed them by subtracting the phonon contribution according to Eq. (15), using the coefficients α and β calculated here.

Our magnetic specific-heat results for $B = 4, 8, 12, 16,$ and 19.5 T are shown in Figs. 5(a)–5(e). The open symbols represent the experimental results for a polydomain sample with

the magnetic field applied along the cubic $\langle 111 \rangle$ direction.²³ The other symbols represent numerical results.

In order to calculate the field-dependent magnetic contribution to the specific heat which would correspond to the experimental results for the polydomain sample, the following simulation was performed. It was assumed that 25% of the domains are oriented in parallel to the direction of the spin chain, and the external magnetic field B is also applied in parallel to the chain direction. For 75% of domains the effective magnetic field

$$B_{\text{eff}} = B \sin(70^\circ)$$

is assumed to be oriented in perpendicular to the direction of the chain. This field generates the uniform field $B^x = B_{\text{eff}} \cos(\theta)$ and the staggered field $B^y = B_{\text{eff}} \sin(\theta)$. Finally, the numerical results include two contributions

$$C/T(B) = 0.75C_{\perp}/T(B_{\text{eff}}) + 0.25C_{\parallel}/T(B). \quad (16)$$

Figures 5(a)–5(e) present the experimental results (open circles) and the numerical results obtained using Eq. (16) (full circles). Each figure also presents the results for the components $0.75C_{\perp}/T(B_{\text{eff}})$ and $0.25C_{\parallel}/T(B)$ of the field directed in perpendicular and parallel direction, respectively. For all values of the magnetic field applied, the results of the present simulations are in good agreement with the experimental values in the whole range of temperatures considered.

The analysis of the energy-gap size on the basis of the specific-heat data is indirect. Since the gap is determined by the staggered field,⁸ its size is related to the position T_{max} of the peaks in the temperature dependence of $C(B)/T$. These positions depend, however, only on the value of the uniform field component B^x , whereas our experimental data for the polydomain sample contain the component C_{\parallel}/T which originates from the chains parallel to the field. This longitudinal component can be estimated numerically and subtracted, yielding the transverse part

$$C_{\perp}/T = C_{\text{exp}}/T - C_{\parallel}/T. \quad (17)$$

The peak positions found from the expression (17) can be related to those following from Fig. 9 of Ref. 8, taking into account that for Yb_4As_3 $J/k_B = -28$ K. From Fig. 9 of Ref. 8 we can find the nonlinear relation between the gap Δ/J and T_{max}/J in the form

$$\Delta/J = a(B_s^y)T_{\text{max}}/J, \quad (18)$$

where

$$\Delta/J = 1.78(g_{\perp}\mu_B B_s^y/J)^{2/3} \cdot |\ln(g_{\perp}\mu_B B_s^y/J)|^{1/6}. \quad (19)$$

Having determined the dependence $a(B_s^y)$, the position T_{max} of the maxima in our $C_{\perp}(B)/T$ can be read out as follows. First we calculate the value B_{eff} for any applied field, next we find B_s^y related to B_{eff} , and then the corresponding value $a(B_s^y)$ which enables estimation of Δ for a given T_{max} .

Figure 6 presents the energy-gap values obtained in this way on the basis of our experimental data (full squares) as a function of $B_{\text{eff}}^{2/3}$. Full circles present the values obtained from the inelastic neutron scattering (INS).¹⁸ In both experiments the energy-gap values found fulfil the power law $B^{2/3}$ and

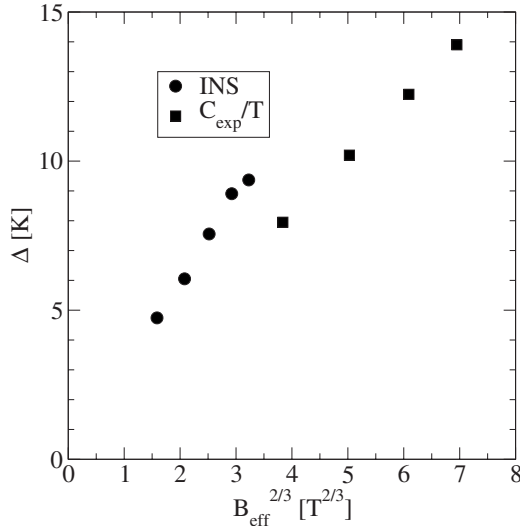


FIG. 6. The energy-gap values as a function of the magnetic field intensity. The experimental results obtained by INS are marked with full circles ($\Delta=2.97B^{2/3}$). The energy gap obtained from the analysis of the specific heat data C/T ($\Delta=2.01B^{2/3}$) is marked by full squares.

confirm the agreement with the field theory predictions for different ranges of fields. However, the slopes of the lines in Fig. 6 are different, indicating different values of the proportionality coefficient $b=\Delta/B^{2/3}$. For the direct INS data $b=2.97 \text{ K T}^{-2/3}$, whereas our specific-heat-based estimation gives $b=2.01 \text{ K T}^{-2/3}$. The latter is closer to $b=1.89 \text{ K T}^{-2/3}$ which can be inferred from Eq. (19) neglecting the logarithmic correction and assuming $J/k_B=-28 \text{ K}$. The gap values derived from INS have been obtained from peak positions in the spectra of the inelastic response at $q=1$ versus energy.¹⁸ Since for a given magnetic field this peak is located beyond the energy at which zero intensity is observed in the spectrum, this analysis should overestimate

the size of the gap, explaining the discrepancy to our estimate of $\Delta(B_{\text{eff}})$.

VII. CONCLUSIONS

The QTM method has been applied to the one-dimensional Heisenberg model with DM interactions in the $S=\frac{1}{2}$ spin chain. New measurements of the specific-heat coefficient of a polydomain sample of Yb_4As_3 have been analyzed. The lattice contribution has been determined using the Bethe ansatz solution for the magnetic specific-heat contribution with an exchange coupling constant of $J/k_B=-28 \text{ K}$.

Next the field-dependent data of the low-temperature specific heat have been reanalyzed, taking into account our estimates of the lattice contribution. It has been shown that the resulting magnetic specific heat can be quantitatively accounted for by the Heisenberg model without additional adjustable parameters. It is also demonstrated that the energy gap develops according to the sine Gordon prediction in the range of the fields applied.

A new approach to the analysis of the QTM simulation results has been proposed, based on the polynomial extrapolation. This approach has significantly improved the accuracy of the simulation results, which permitted getting reliable numerical results for temperatures lower than those hitherto considered within QTM, fully consistent with those known from the Bethe ansatz and DMRG calculations. We observed that the variation in the data decreases with increasing degree of the extrapolation polynomial k and the reliability of the estimates increases for $k \geq 4$.

ACKNOWLEDGMENTS

This work was supported by the Polish Ministry of Science and High Education under Grant No. N202 309835 and the UE NoE project under Project No. NMP3-CT-2005-515767. Computations were partially performed on PCSN supercomputing platforms and on the local cluster pearl.

*r.matysiak@eti.uz.zgora.pl

†gjk@amu.edu.pl

¹M. Hase, I. Terasaki, and K. Uchinokura, Phys. Rev. Lett. **70**, 3651 (1993).

²D. C. Johnston, R. K. Kremer, M. Troyer, X. Wang, A. Klümper, S. L. Budko, A. F. Panchula, and P. C. Canfield, Phys. Rev. B **61**, 9558 (2000).

³F. D. M. Haldane, Phys. Rev. Lett. **50**, 1153 (1983).

⁴P. Renard, M. Verdagner, L. P. Regnault, W. A. C. Erkelens, J. Rossat-Mignat, J. Ribas, W. G. Stirling, and C. Vettier, J. Appl. Phys. **63**, 3538 (1988).

⁵M. Oshikawa and I. Affleck, Phys. Rev. Lett. **79**, 2883 (1997).

⁶J. C. Bonner and M. E. Fisher, Phys. Rev. **135**, A640 (1964).

⁷T. Delica and H. Leschke, Physica A **168**, 736 (1990).

⁸N. Shibata and K. Ueda, J. Phys. Soc. Jpn. **70**, 3690 (2001).

⁹D. C. Johnston, R. K. Kremer, M. Troyer, X. Wang, A. Klümper, S. L. Bud'ko, A. F. Panchula, and P. C. Canfield, Phys. Rev. B

61, 9558 (2000).

¹⁰G. Kamieniarz, M. Bieliński, and J.-P. Renard, Phys. Rev. B **60**, 14521 (1999).

¹¹A. Ochiai, T. Suzuki, and T. Kasuya, J. Phys. Soc. Jpn. **59**, 4129 (1990).

¹²M. Köppen, M. Lang, R. Helfrich, F. Steglich, P. Thalmeier, B. Schmidt, B. Wand, D. Pankert, H. Benner, H. Aoki, and A. Ochiai, Phys. Rev. Lett. **82**, 4548 (1999).

¹³M. Kohgi, K. Iwasa, A. Ochiai, T. Suzuki, J.-M. Mignot, B. Gillon, A. Gukasov, J. Schweizer, K. Kakurai, M. Nishi, A. Döni, and T. Osakabe, Physica B **230-232**, 638 (1997).

¹⁴V. N. Antonov, A. N. Yaresko, A. Ya. Perlov, P. Thalmeier, P. Fulde, P. M. Oppeneer, and H. Eschrig, Phys. Rev. B **58**, 9752 (1998).

¹⁵M. Kohgi, K. Iwasa, J.-M. Mignot, A. Ochiai, and T. Suzuki, Phys. Rev. B **56**, R11388 (1997).

¹⁶B. Schmidt, H. Aoki, T. Cichorek, J. Custers, P. Gegenwart, M.

- Kohgi, M. Lang, C. Langhammer, A. Ochiai, S. Paschen, F. Steglich, T. Suzuki, P. Thalmeier, B. Wand, and A. Yaresko, *Physica B* **300**, 121 (2001).
- ¹⁷P. Fulde, B. Schmidt, and P. Thalmeier, *Europhys. Lett.* **31**, 323 (1995).
- ¹⁸M. Kohgi, K. Iwasa, J.-M. Mignot, B. Fak, P. Gegenwart, M. Lang, A. Ochiai, H. Aoki, and T. Suzuki, *Phys. Rev. Lett.* **86**, 2439 (2001).
- ¹⁹D. C. Dender, P. R. Hammar, D. H. Reich, C. Broholm, and G. Aeppli, *Phys. Rev. Lett.* **79**, 1750 (1997).
- ²⁰R. Feyerherm, S. Abens, D. Günther, T. Ishida, M. Meißner, M. Meschke, and T. Nogami, *J. Phys.: Condens. Matter* **12**, 8495 (2000).
- ²¹M. Oshikawa and I. Affleck, *Phys. Rev. Lett.* **82**, 5136 (1999).
- ²²S. Bertaina, V. A. Pashchenko, A. Stepanov, T. Masuda, and K. Uchinokura, *Phys. Rev. Lett.* **92**, 057203 (2004).
- ²³P. Gegenwart, H. Aoki, T. Cichorek, J. Custers, N. Harrison, M. Jaime, M. Lang, A. Ochiai, and F. Steglich, *Physica B* **312-313**, 315 (2002).
- ²⁴G. Kamieniarz, R. Matysiak, P. Gegenwart, H. Aoki, and A. Ochiai, *J. Magn. Magn. Mater.* **290-291**, 353 (2005).
- ²⁵M. Oshikawa, K. Ueda, H. Aoki, A. Ochiai, and M. Kohgi, *J. Phys. Soc. Jpn.* **68**, 3181 (1999).
- ²⁶H. Shiba, K. Ueda, and O. Sakai, *J. Phys. Soc. Jpn.* **69**, 1493 (2000).
- ²⁷H. A. Bethe, *Z. Phys.* **71**, 205 (1971).